Supporting Information

Data-Based Modeling, Multi-objective Optimization and Multi-criteria Decision Making of a Catalytic Ozonation Process for Degradation of a Colored Effluent

Seyed Reza Nabavi[1]*, Saheleh Ghahri[2] and Gade Pandu Rangaiah[3, 4]*

1 Department of Applied Chemistry, Faculty of Chemistry, University of Mazandaran, 4741695447 Babolsar, Iran; srnabavi@umz.ac.ir

2 Department of Applied Chemistry, Faculty of Chemistry, University of Mazandaran, 4741695447 Babolsar, Iran; ghahri_sh@gmail.com

3 Department of Chemical and Biomolecular Engineering, National University of Singapore, Singapore 117585, Singapore; chegpr@nus.edu.sg

4 School of Chemical Engineering, Vellore Institute of Technology, Vellore 632014, India.

* Correspondence: S.R Nabavi, srnabavi@umz.ac.ir; G.P Rangaiah, chegpr@nus.edu.sg

S.1. Characterization of Catalysts

The crystalline structures of Fe_3O_4 nanoparticles were confirmed by X-ray diffraction analysis (XRD) patterns (**Figure S1**). The crystal structure of Fe_3O_4 nanoparticles was corroborated by the presence of diffraction peaks at $2\theta = 30.45^o$, 35.7^o, 45.46^o, 53.82^o, 57.37^o, 62.9^o, 70^o and 75^o, which can be assigned to the (220), (311), (400), (422), (511), (440), (620) and (533) crystal planes of face-centered cubic Fe_3O_4 (Guo et al., 2012).

Fourier-transform infrared spectroscopy (FTIR) spectra of Fe_3O_4 nanoparticles are shown in **Figure S2**. The broad peak between 600 and 579 cm^{-1} corresponds to the vibration of M_T-O-M_O for Fe_3O_4, where M_T and M_O denote the metal occupying tetrahedral and octahedral positions, respectively (Karaagac et al., 2010).

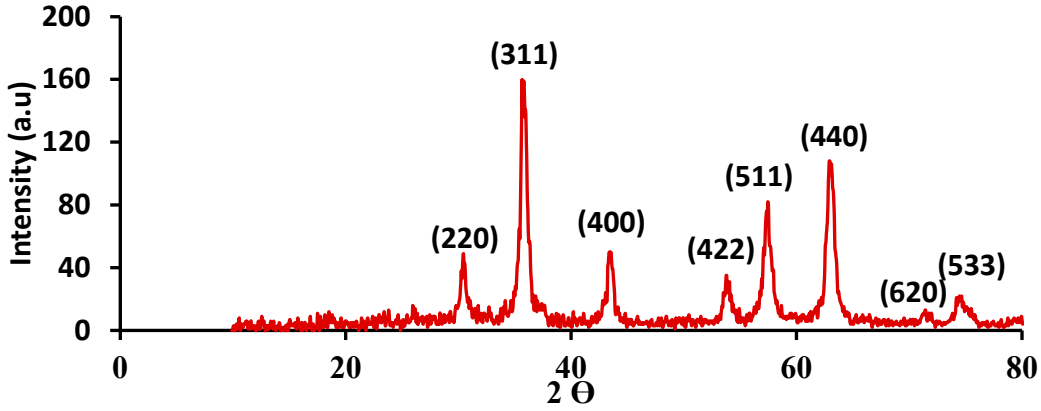

Figure S1. XRD patterns of Fe_3O_4 nanoparticles.

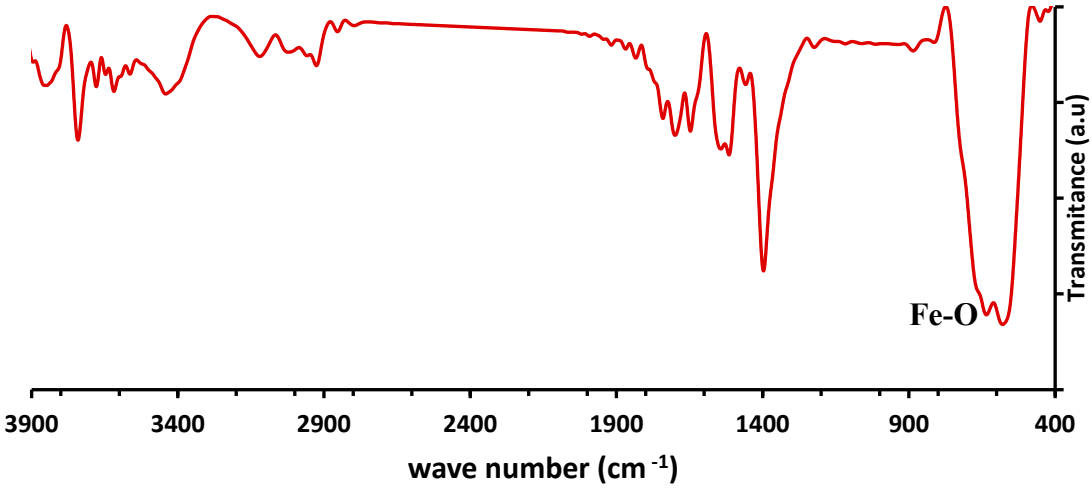

Figure S2. FTIR spectra of mesoporous Fe_3O_4.

The N_2 adsorption–desorption isotherms and the Barrett–Joyner–Halenda (BJH) plot for Fe_3O_4 are given in **Figure S3**. The data obtained using Brunauer–Emmett–Teller (BET), BJH and t-plot models are summarized in **Table S1**. Accordingly, the total specific surface area measurements for Fe_3O_4, obtained with the BET model and the t-plot, are in good agreement with each other. The closeness of the calculated data can be used to confirm the accuracy of specific surface area measurements (Ghadamnan et al., 2019). In **Figure S3a**, a hysteresis loop appeared in the Fe_3O_4 nanoparticles, indicating that the synthesized nanoparticles have a mesoporous structure. **Figure S3b** and the data calculated from the BJH model (V_m = 0.092 cm^3/g and a_m = 60.5 m^2/g) in **Table S1** also confirm this claim. The mesoporous structure of

Fe_3O_4 nanoparticles can be attributed to the space between the condensed nanoparticles due to their strong magnetic interactions (Vinodha et al., 2019). This mesoporous structure is favorable for ozone mass transfer and AR88 adsorption on the catalyst surface, which in turn increases the degradation rate of AR88.

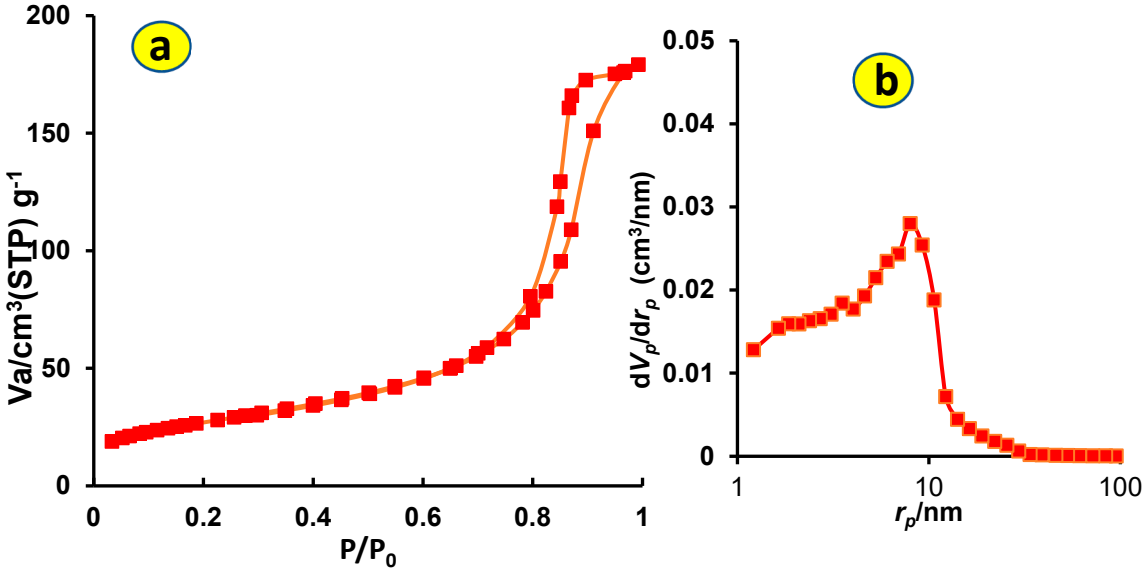

Figure S3. (a) N_2 adsorption–desorption isotherms and **(b)** BJH plot for Fe_3O_4 nanoparticles.

Table S1. Porosity data obtained from BET, BJH and t-plot for mesoporous Fe_3O_4 nanoparticles.

	Specification	Fe_3O_4
BET	Total specific surface area (S_{BET}, m^2g^{-1})	90.0
	Total pore volume (V_p, cm^3g^{-1})	0.110
	Mean pore diameter (nm)	4.8
t-Plot	Total specific surface area (a_1, m^2g^{-1})	91.7
	External specific surface area (a_2, m^2g^{-1})	20.59
	Micropore area (a_1- a_2, m^2g^{-1})	71.15
	Micropore volume (V_p, cm^3g^{-1})	0.062
BJH	Mesopore volume (V_{pm}, cm^3g^{-1})	0.092
	Mesopore area (a_{mp}, m^2g^{-1})	60.5
	Mesopore distribution peak (r_p, nm)	1.2

Figure S4 illustrates the field emission scanning electron microscopy (FESEM) image of Fe_3O_4 and its corresponding energy-dispersive X-ray spectroscopy (EDS) spectrum. The FESEM image of Fe_3O_4 nanoparticles indicates that the particles are often spherical; although they are in nanoscale, they are visible in some regions of aggregation. The histogram of the nanoparticle diameter distribution is shown as an inset in **Figure S4(a)**. The prepared nanoparticles have a diameter range of 10-50 nm and an average diameter of 28 nm.

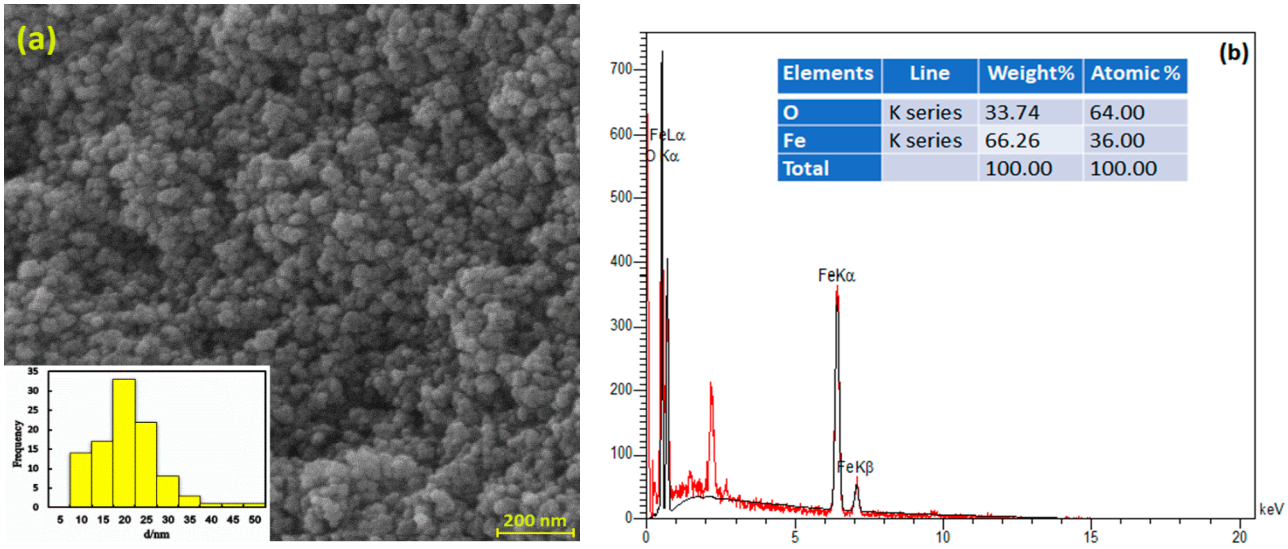

Figure S4. FESEM image (a) and EDS spectrum (b) of Fe_3O_4 nanoparticles.

A comparison of the degradation efficiency with that of other processes reported in the literature is shown in Table S2. Although high %DE has been reported in these processes, the initial concentration of AR88 is lower than the value tested in this study. In addition, the time required to reach these high levels of %DE is much higher than that elapsed in the present study.

Table S2. Comparison of the degradation efficiency (DE%) of AR88 by COP with that of other processes in the literature.

Process	Initial concentration (ppm)	Reaction time (h)	DE%	Reference
Biological	100	12	98	(Khehra et al., 2006)
Photocatalyst	20	0.5	94	(Bahram et al., 2017)
Adsorption–Photocatalyst	40	5	100	(Gao et al., 2011)
COP (O_3/Fe_3O_4)	150	0.5	71.1	This work

References

Bahram, M., Salami, S., Moghtader, M., Moghadam, P. N., Fareghi, A. R., Rasouli, M., & Salimpour, S. (2017). Photocatalytic degradation of anionic azo dyes Acid Orange 7 and Acid Red 88 in aqueous solutions using Tio2-containing hydrogel. *Analytical and Bioanalytical Chemistry Research*, *4*(1). https://doi.org/10.22036/abcr.2017.41098

Gao, B., Yap, P. S., Lim, T. M., & Lim, T. T. (2011). Adsorption-photocatalytic degradation of Acid Red 88 by supported TiO2: Effect of activated carbon support and aqueous anions. *Chemical Engineering Journal*, *171*(3). https://doi.org/10.1016/j.cej.2011.05.006

Ghadamnan, E., Nabavi, S. R., & Abbasi, M. (2019). Nano LTA Zeolite in Water Softening Process: Synthesis, Characterization, Kinetic studies and process optimization by Response Surface Methodology (RSM). *J. Water Environ. Nanotechnol*, *4*(2).

Guo, S., Wu, H., Gao, G., Zhou, X., & Zhang, Y. (2012). Control on the formation of Fe3O4 nanoparticles on chemically reduced graphene oxide surfaces. *CrystEngComm*, *14*(2). https://doi.org/10.1039/c1ce05724c

Karaagac, O., Kockar, H., Beyaz, S., & Tanrisever, T. (2010). A simple way to synthesize superparamagnetic iron oxide nanoparticles in air atmosphere: Iron ion concentration effect. *IEEE Transactions on Magnetics*, *46*(12). https://doi.org/10.1109/TMAG.2010.2076824

Khehra, M. S., Saini, H. S., Sharma, D. K., Chadha, B. S., & Chimni, S. S. (2006). Biodegradation of azo dye C.I. Acid Red 88 by an anoxic - Aerobic sequential bioreactor. *Dyes and Pigments*, *70*(1). https://doi.org/10.1016/j.dyepig.2004.12.021

Vinodha, G., Shima, P. D., & Cindrella, L. (2019). Mesoporous magnetite nanoparticle-decorated graphene oxide nanosheets for efficient electrochemical detection of hydrazine. *Journal of Materials Science*, *54*(5). https://doi.org/10.1007/s10853-018-3145-z